UC Irvine
UC Irvine Electronic Theses and Dissertations

Title

Flexure Design for Eight-Bar Rectilinear Motion Mechanism

Permalink

https://escholarship.org/uc/item/6f276063

Author

Liu, Yang

Publication Date

2015

Peer reviewed|Thesis/dissertation

UNIVERSITY OF CALIFORNIA,
IRVINE

Flexure Design for Eight-Bar Rectilinear Motion Mechanism

THESIS

submitted in partial satisfaction of the requirements
for the degree of

MASTER OF SCIENCE

in Mechanical and Aerospace Engineering

by

Yang Liu

Thesis Committee:
Professor J. Michael McCarthy, Chair
Professor Kenneth D. Mease
Professor Lorenzo Valdevit

2015

DEDICATION

To my parents,
thank you for your love and support.

TABLE OF CONTENTS

LIST OF FIGURES

LIST OF TABLES

ACKNOWLEDGMENTS

CURRICULUM VITAE

Yang Liu

EDUCATION

Master of Science in Mechanical and Aerospace Engineering   **2015**
University of California, Irvine   *Irvine, California*

Bachelor of Science in Mechanical Engineering   **2011**
Beijing Institute of Technology   *Beijing, China*

RESEARCH EXPERIENCE

Graduate Research Assistant   **2013–2015**
University of California, Irvine   *Irvine, California*

TEACHING EXPERIENCE

Teaching Assistant   **2013–2015**
University of California, Irvine   *Irvine, California*

PROFESSIONAL MEMBERSHIPS

American Society of Mechanical Engineers (ASME)

ABSTRACT OF THE DISSERTATION

Flexure Design for Eight-Bar Rectilinear Motion Mechanism

By

Yang Liu

Master of Science in Mechanical and Aerospace Engineering

University of California, Irvine, 2015

Professor J. Michael McCarthy, Chair

This thesis replaces the hinged pivots of an eight-bar linkage with flexure joints in order to achieve a flexure-connected linkage system that guides rectilinear movement of its end-effector. The goal is a linkage design that can be reduced in size to provide a suspension for the proof masses of a MEMS gyroscope. The symmetric design of the linkage and its long travel relative to other MEMS suspensions has the potential to provide a number of advantages, such as the reduction of quadrature error. The design presented yields 0.1% deviation over its range of movement. An example also presents the driving linkage of the MEMS gyroscope, which is also designed as flexure connected linkage.

Chapter 1

Introduction

1.1 Rectilinear Eight-bar Compliant Mechanism

This thesis presents an eight-bar linkage in which the hinged pivots have been replaced by flexures in order to guide the rectilinear movement of a MEMS gyroscope. The flexure-connected eight-bar linkage provides a long-travel rectilinear suspension for the proof masses in the MEMS gyroscope, which reduces quadrature error.

Existing rectilinear motion linkages have 10 bars, see Kempe (1877)[6]. Our goal is an eight-bar linkage that guides rectilinear movement with low error and with no link overlap so the hinged joints can be replaced with flexures. A flexure allows movement through bending of its elements. An example of application of flexure pivots can be seen from a 2-DOF flexure parallel mechanism [10].

The resulting flexure-connected eight-bar linkage has dimensions of approximately $200mm \times 150mm$ and provides 33mm rectilinear movement with a maximum deviation of 0.1%.

1.2 Literature Review

Suspensions for MEMS gyroscope are usually formed from springs, such as the *Crab-leg spring, U-spring, Serpentine spring and Folded-flexure spring* (2006)[11]. These suspensions are asymmetric, which introduces in quadrature error. Shi et al. (2006)[11] provide design principles to reduce quadrature error.

Our research provides another approach by designing a symmetric eight-bar and introducing flexures as the pivots, in order to obtain a compliant mechanism that provides a rectilinear movement. The symmetric structure of this suspension results in high-rate sensitivity and low temperature dependent drift [1]. In addition, it provides a long travel rectilinear movement of the proof mass.

The synthesis of an eight-bar linkage to reach five task positions has been presented by Soh and McCarthy (2007)[12] and Sonawale and McCarthy (2014)[13]. This method starts from two 3R chain robots and by adding two RR constraints to get one degree-of-freedom eight-bar linkage. In this research, we follow this procedure and obtain a number of eight-bar linkages from which we chose the designs with non-overlapping links. This provides a simple way to introduce flexures into the linkage.

Eight-bar linkages that have pivots replaced by flexures are examples of compliant mechanisms. Compliant mechanisms have proven to have a wide range of applications both in MEMS devices and larger scale systems, [2] [7]. Howell [4, 5] presents the design rules for the introduction of flexures in traditional pivoted linkage systems. The analysis of beam flexure performance had been presented by Awtar and Slocum (2007)[3]. In this paper, we replace the hinges in our eight-bar linkage design with long-thin beam flexures, analyze the resulting system, and adjust the flexure dimensions to ensure performance.

Chapter 2

Straight-Line Mechanism

An important part of traditional mechanism design is to generate straight-line motion. Mc-Carthy [9] and Kempe [6] have talked about some existing straight-line mechanisms. These straight-line motion mechanisms are summarized in the following sections.

2.1 Watt's Linkage
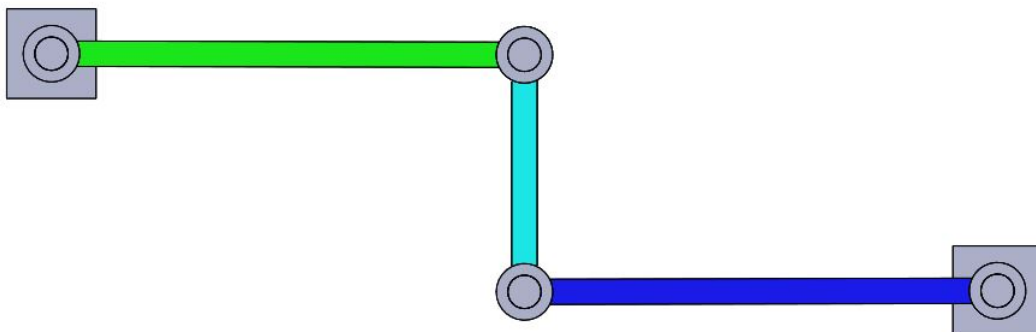
Figure 2.1: SOLIDWORKS MODEL OF WATT'S LINKAGE.
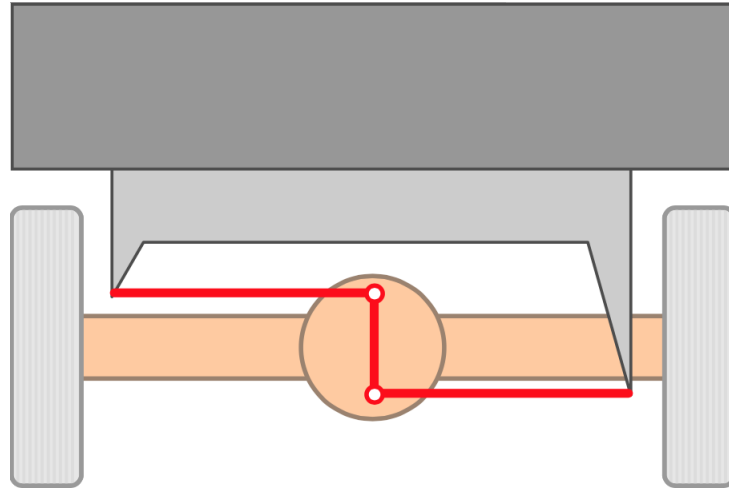
Figure 2.2: WATT'S LINKAGE USED AS THE AUTOMOBILE'S REAR WHEEL SUS-PENSION 1.

Figure 2.3: WATT'S LINKAGE USED AS THE AUTOMOBILE'S REAR WHEEL SUS-PENSION 2.

The best known straight-line linkage is the watt parallel linkage. James Watt developed this approximate straight-line linkage in 1784 to guide the piston of the early engines. It is also used on the automobile suspensions to allow the axle moving in vertical direction while at the same time preventing the sideway movement. The SolidWorks model of Watt's linkage can be seen in Fig2.1 and an application of Watt linkage as a suspension on the rear axle of

a car can be seen in Fig.2.2 and Fig.2.3.
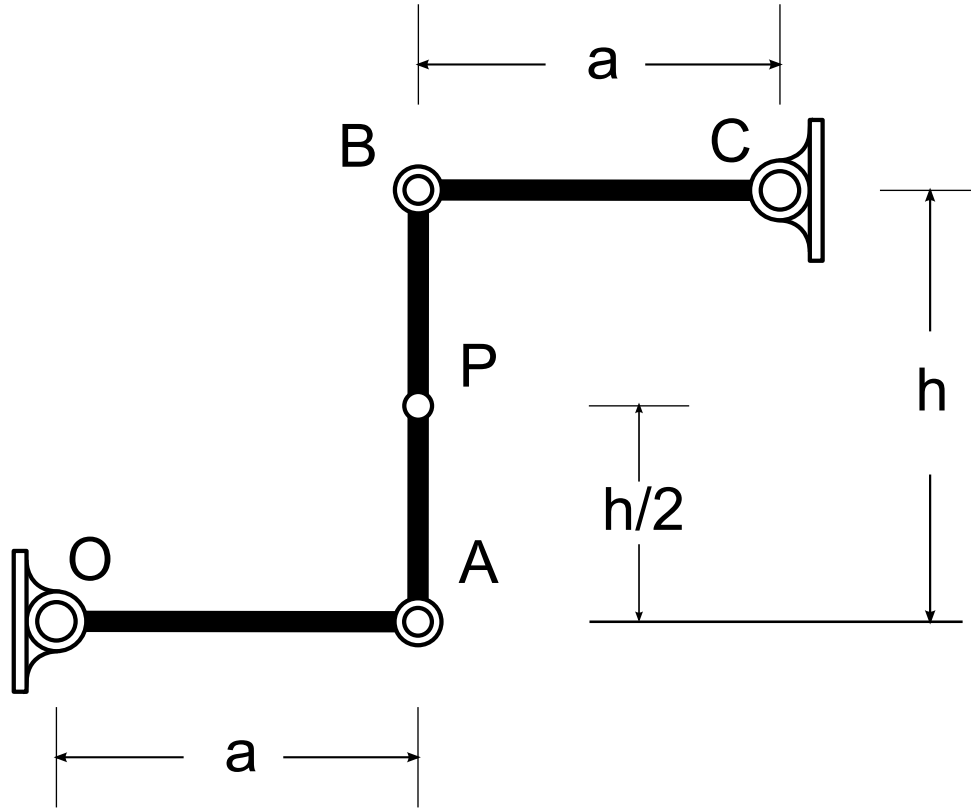
Figure 2.4: THE DIMENSIONS OF WATT'S LINKAGE.

Watt linkage is consisting of four links if the ground link is counted. So it is basically a four-bar linkage. The tracing point P is on the coupler link. It has a distance x measured from point A. Let us label the link length as $|OA| = a, |BC| = b, |AB| = h$ and $|OC| = g$. The tracing point P follow an approximate straight line along a part of its path if the link length OA and BC satisfy the relationship that $x/(h - x) = a/b$ and the ground link has length $g^2 = h^2 + (a + b)^2$. The drawing of Watt's linkage can be seen in Fig.2.4.

5
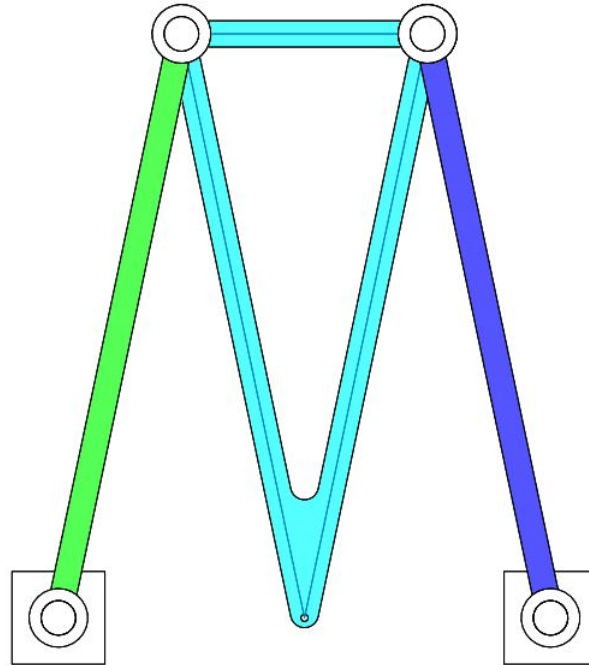
Figure 2.5: SOLIDWORKS MODEL OF ROBERT'S LINKAGE.

2.2   Robert's Linkage

The straight line described by Watt's linkage is sufficiently accurate but it is still not a perfect straight line. The Robert's linkage is a closer approximation of straight line than Watt's linkage. The SolidWorks model of Robert's linkage can be seen in Fig.2.5

The link lengths of Robert's linkage satisfy the relationship that $a = b$ and $g = 2h$. The tracing point P is at the position making a isosceles triangle structure and with the length $|AP| = |AO| = a$ and $|BP| = |BC| = b$. The result is the tracing point P can move in a nearly straight line. The configuration of Robert's linkage can be seen in Fig.2.6.
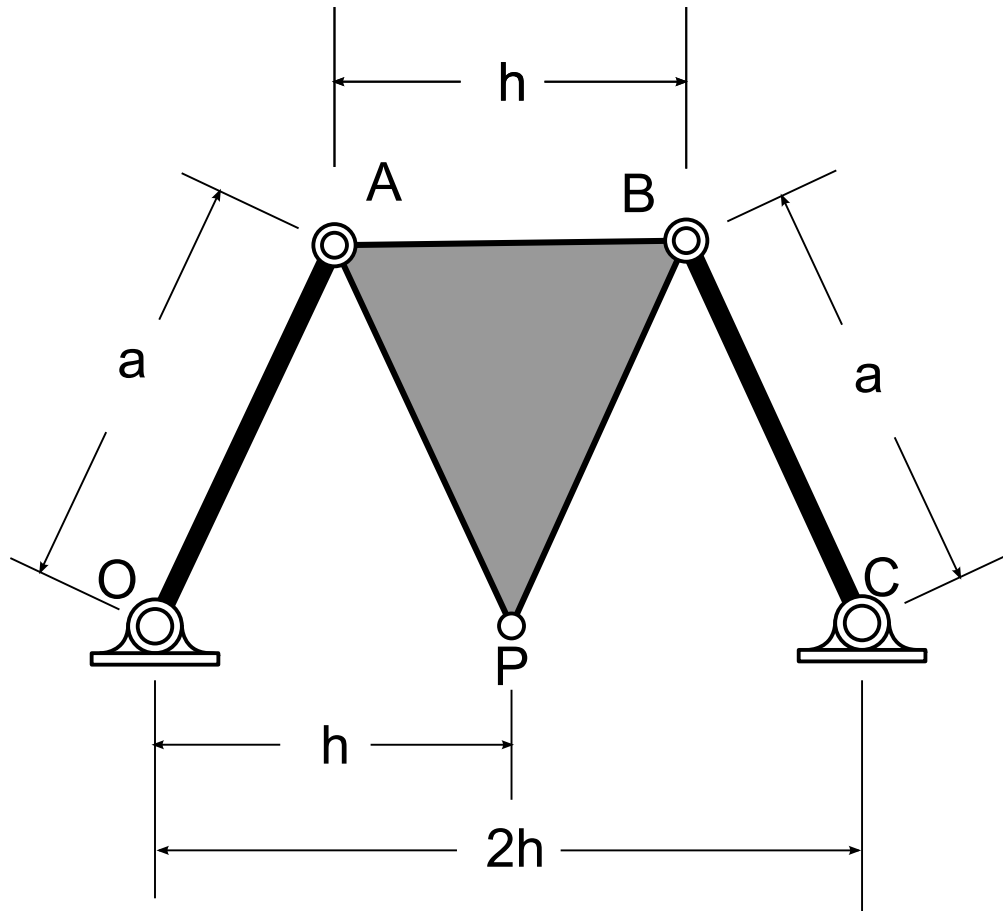
Figure 2.6: THE DIMENSIONS OF ROBERT'S LINKAGE.

2.3 Chebyshev's Linkage

Another straight-line mechanism was invented by the 19th mathematician Pafnuty Cheby-shev. It is called the Chebyshev's linkage which can convert the rotational motion to ap-proximate straight line motion. The SolidWorks model of Chebyshev's linkage is in Fig.2.7.

The Chebyshev's linkage has a specific dimension to make the tracing point P move in a straight line. The ground link $|OC| = 2h$, the coupler link length is $|AB| = h$ and the input link and output link have the same length $|OA| = |BC| = 2.5h$. The tracing point P is set at the middle of the coupler link. The configuration of the CHebyshev's linkage can be seen in Fig.2.8.
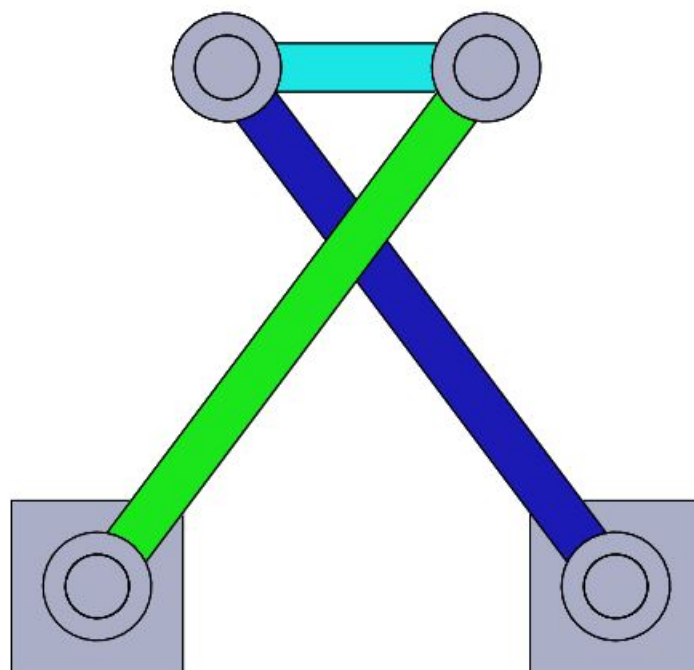
Figure 2.7: SOLIDWORKS MODEL OF CHYBYSHEV'S LINKAGE.
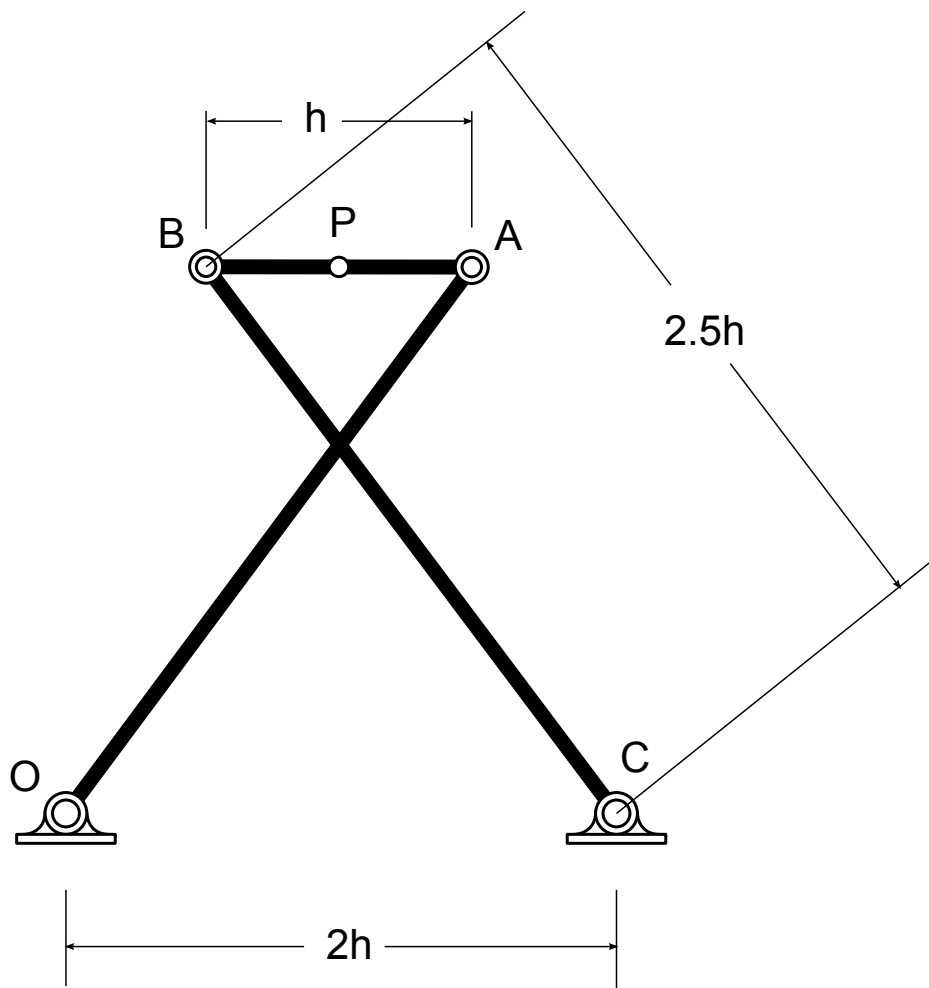
Figure 2.8: THE DIMENSIONS OF CHEBYSHEVE'S LINKAGE.

2.4 Peaucellier–Lipkin Linkage
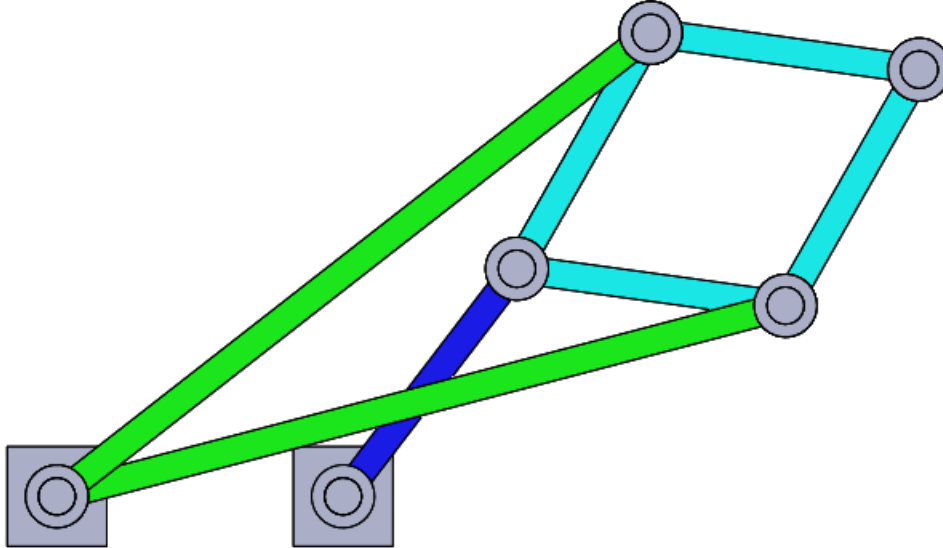
Figure 2.9: SOLIDWORKS MODEL OF PEAUCELLIER'S LINKAGE.

The four-bar linkage can not achieve a perfect straight-line motion. If we want to describe a definite motion curve, we have to use more links. M. Peaucellier firstly invented a mechanism that can achieve strict straight line in 1864 which is eighty years after Watt's linkage. The SolidWorks model of Peaucellier–Lipkin linkage can be seen in Fig.2.9. It is actually an eight-bar linkage if the ground link is counted.

The dimensions of Peaucellier–Lipkin linkage can be seen in Fig.2.10. The link dimensions of the Peaucellier–Lipkin linkage have the relationship that $|OA| = |OD| = a$, $|AB| = |BD| = |DC| = |CA| = b$ and $|OQ| = |QC| = c$. The two long links OA and OD are pivoted at a same fixed point O. The four short links AB, BD, DC and CA formulate a rhombus. The other end of the long link is pivoted to a different vertex of the rhombus as you can see from the figure. These six links formulate a "Peaucellier cell". Then we need an additional link to make the whole mechanism fixed. One end of the additional link is fixed on ground and
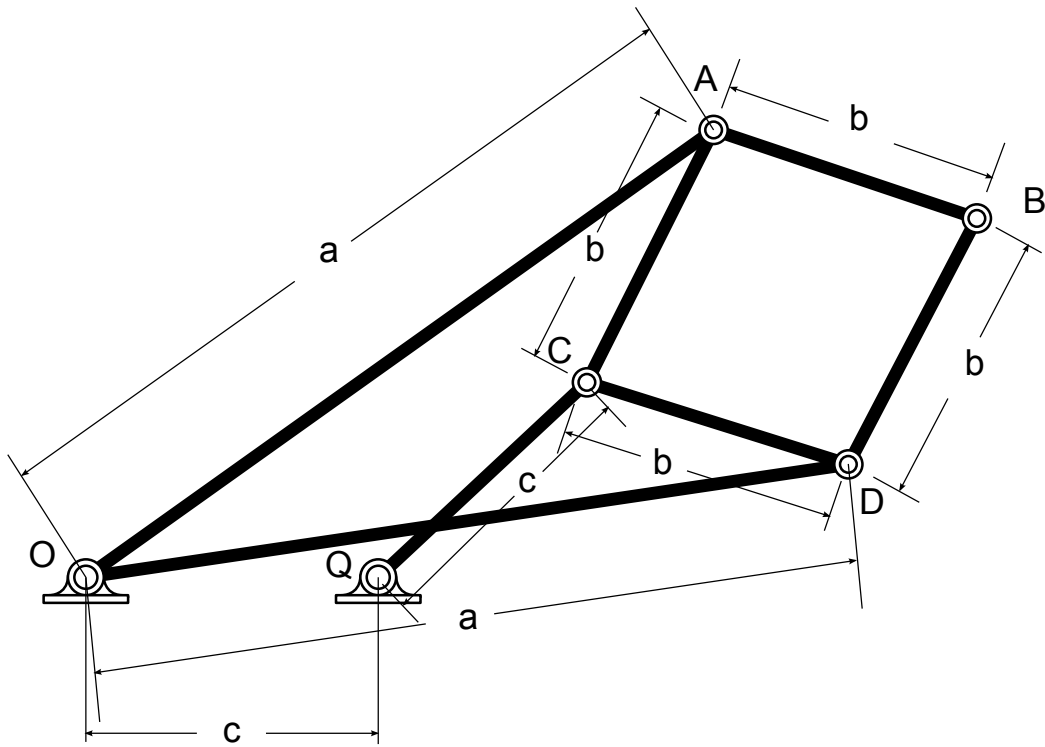
Figure 2.10: THE DIMENSIONS OF PEAUCELLIER'S LINKAGE.
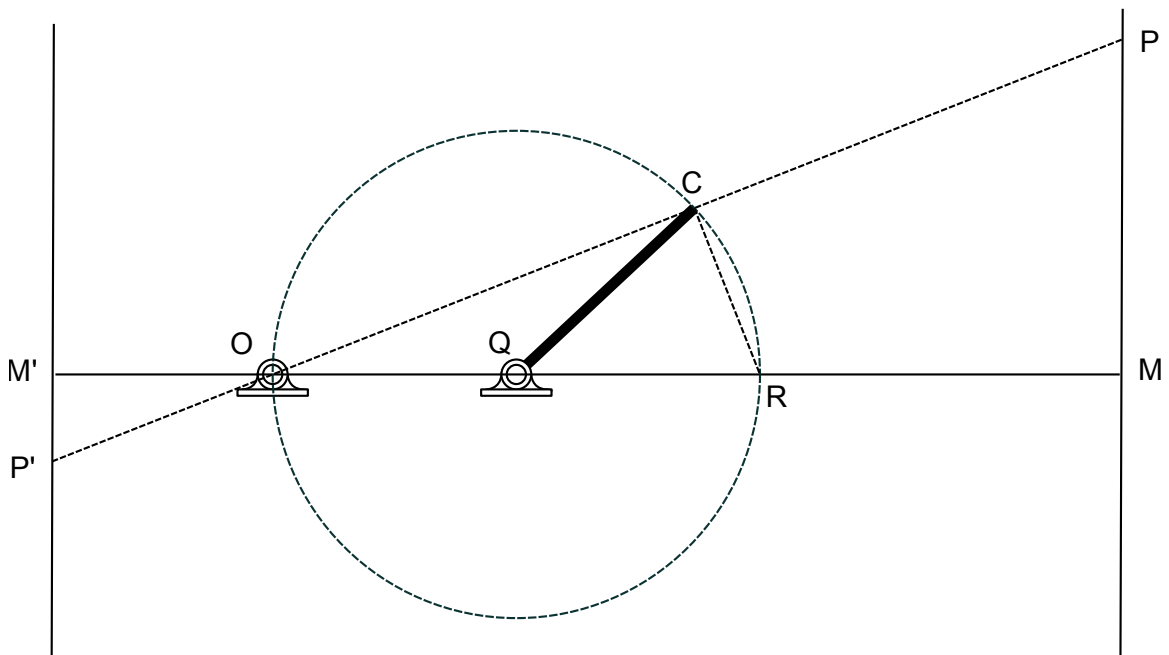
Figure 2.11: THE GEOMETRY OF PEAUCELLIER'S LINKAGE.

the other end is attached to the third vertex of the rhombus. The first ground point and the second ground point are placed on a horizontal line. And the distance of the two ground pivots is equal to the length of the extra link. Then the other free vertex of the rhombus will go through an accurate straight line.

Now let us look at the geometry of the Peaucellier–Lipkin linkage so we can understand the principle of this mechanism. In Fig.2.11, we denote the ground pivot as O and Q which are the same as in Fig.2.10. Here QC is the extra link. Because the ground pivot distance is equal to the extra link's length, so we can draw a circle go through O and C with the center at Q. Points M, M', O and Q are in a same horizontal line. And P, P', O, and C are in a same straight line. We have another relation that $P'M'$ and PM are both orthogonal to the horizontal line $M'OQM$. The triangle OCR is located in a circle so that OCR is a rectangle. From the above, we know the triangle OCR is similar to the triangle OMP. And we have the relation between the sides of the two similar triangle which is as following:

$$OC : OM = OR : OP \tag{2.1}$$

Therefore,

$$OC \cdot OP = OM \cdot OR \tag{2.2}$$

As long as C moves on a circle, OCR will be a rectangle. In addition, the triangle OCR and OMP are sharing a same angle COR or MOP, so the two rectangle triangles will always be similar. Since OR and OM are constants, their multiplication will be a constant. From 2.2, we know $OC \cdot OP$ will be a constant. So when C is moving along the circle, P will always move on a perfect straight line PM which is perpendicular to OQ.

We can also find that if we take the point P to the other side of O. We denote it as P'. In

this case, the triangle OCR and OMP are similar. We can get the same conclusion that:

$$OC : OM' = OR : OP' \tag{2.3}$$

Similar, we get

$$OC \cdot OP' = OM' \cdot OR \tag{2.4}$$

So we get the same conclusion that, for the other side, we have P' move along a vertical straight line.
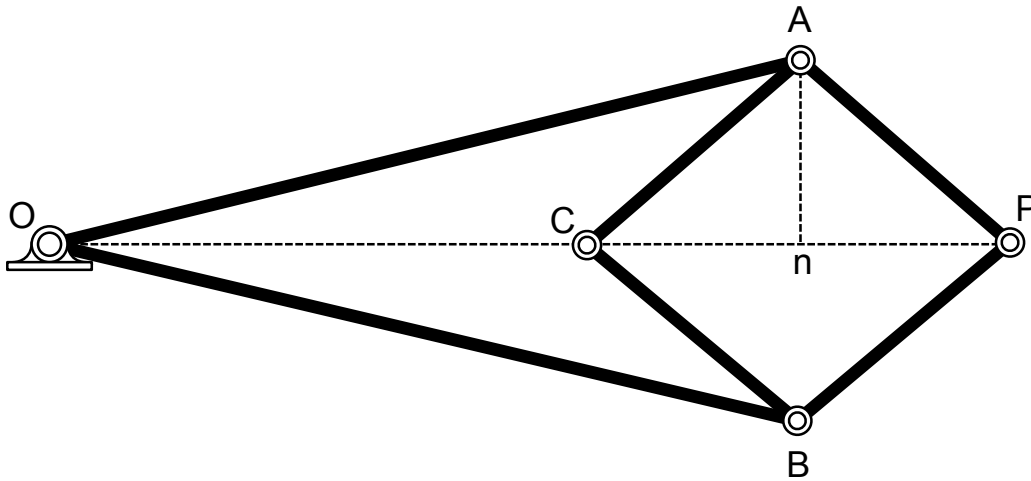
Figure 2.12: THE STRUCTURE OF PEAUCELLIER CELL.

From geometric view, we have proved that if $OC \cdot OP$ is a constant and point O, C and P are on a straight line then P can move in a vertical straight line which is perpendicular to OQ. Also we need constraint C to let it move along a circle. So now our task is to find a mechanism that can make sure O, C and P in a straight line and the relationship of these three points always satisfies $OC \cdot OP$ is a constant. Let us verify whether the Peaucellier cell satisfy our requirements. We draw the structure of a Peaucellier cell in Fig2.12. We already know $ACBP$ is a rhombus and OA and OB are equal length. From the symmetry of the Peaucellier cell, we can know the point O, C and P will always lie on a straight line. So the

first condition is satisfied. Now let us verify if the second condition is satisfied. We draw a imaginary line An that is perpendicular to CP. We know from the property of the rhombus that the length of Cn is equal to Pn. So we have

$$OA^2 = On^2 + An^2 \tag{2.5}$$

and

$$AP^2 = Pn^2 + An^2 \tag{2.6}$$

Subtract equation (2.7) from equation (2.8), we get

$$OA^2 - AP^2 = On^2 - Pn^2$$
$$= [On - Pn] \cdot [On + Pn]$$
$$= OC \cdot OP$$

Since OA and AP are both constants leading to $OC \cdot OP$ is always a constant. We have proved that the second condition is satisfied. There are two elements to compose a Peaucellier linkage: the Peaucellier cell and the extra link. If we make the point O, C in Fig.2.12 coincide with the points in Fig.2.11 and an extra link constraint point C to move on a circle, the point P will go through a perfect straight line.

2.5 Modified Peaucellier–Lipkin Linkage

Once we know the principle of designing a Peaucellier linkage, we can design another form of Peaucellier linkage which can make the point P' move in a straight line on the other side of fixed ground pivot in Fig.2.11. If we take the farthest and nearest two neighboring sides

14

of the rhombus in the Peaucellier link away respectively, we get two four-bar mechanisms. The one named "kite" is showing in Fig.2.13, and the other named "spear head" is showing in Fig.2.14.

Because the kite and spear head mechanisms are both part of the same Peaucellier linkage, so the long links and short links in the kite and spear head mechanism are equal length. If we place one on the top of the other and make the long links coincide, we get exactly the Peaucellier cell showing in Fig.2.12. If we keep the angles between the long links and the short links the same for both kite and spear head mechanism and make the short links
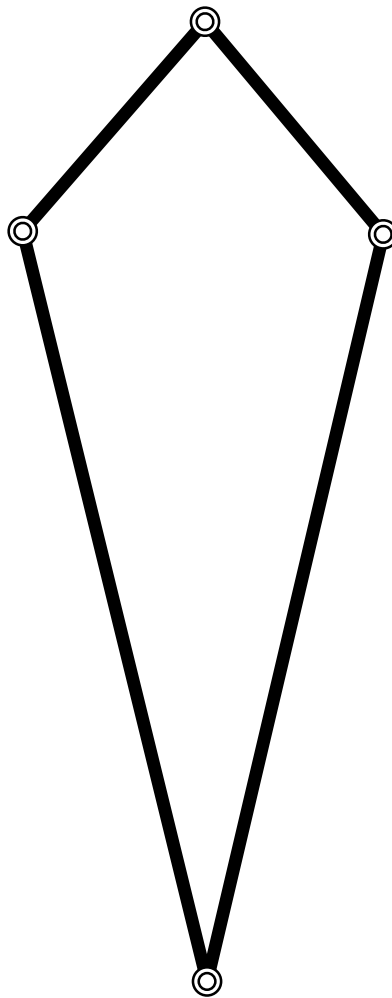
Figure 2.13: THE STRUCTURE OF KITE MECHANISM.
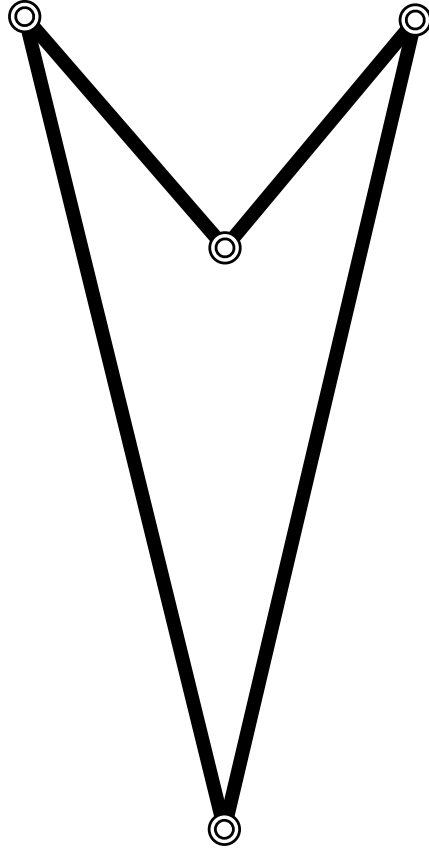
Figure 2.14: THE STRUCTURE OF SPEAR HEAD MECHANISM.
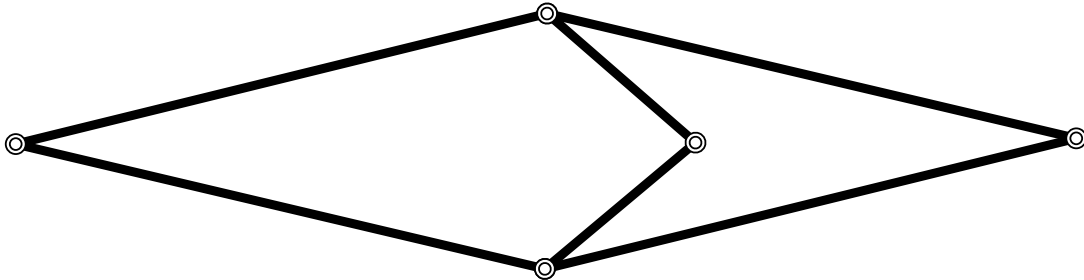
Figure 2.15: THE MODIFIED PEAUCELLIER LINKAGE.

coincide, we get the modified Peaucellier linkage. This is showing in Fig.2.15.

The symmetric structure of the modified Peaucellier linkage makes the three pivots in the middle always lie in a straight line. So the first condition is satisfied. The second condition still need to be proved. We already proved the multiplication of the height of kite and spear

16
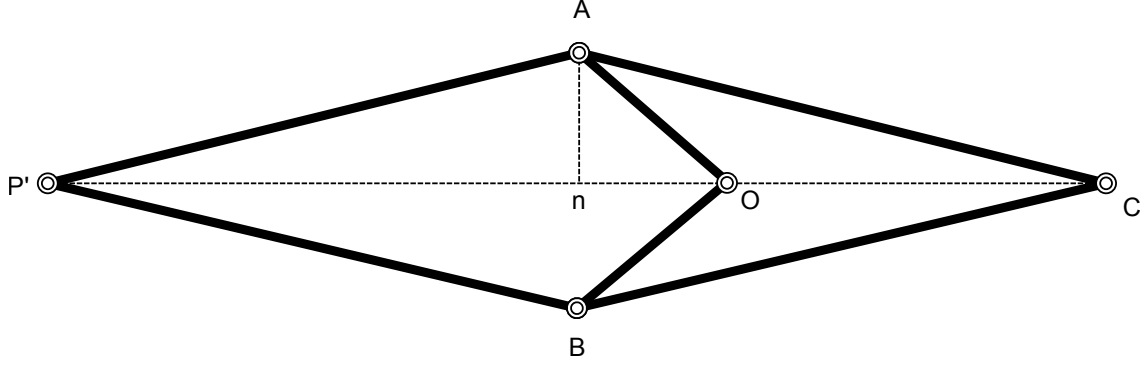
Figure 2.16: THE STRUCTURE OF THE PEAUCELLIER LINKAGE.

head mechanism is a constant. We use the similar method showing in Fig.2.12 to prove the second condition for the modified peaucellier mechanism. We also draw an imaginary line An which is perpendicular to $P'C$. The drawing is showing in Fig2.16. We find the similar relationship between the link lengths as following:

$$OA^2 = On^2 + An^2 \tag{2.7}$$

and

$$AP'^2 = P'n^2 + An^2 \tag{2.8}$$

Subtract equation (2.7) from equation (2.8), we get

$$OA^2 - AP'^2 = On^2 - P'n^2$$
$$= [On - P'n] \cdot [On + P'n]$$
$$= OC \cdot OP'$$

Because the length of link OA and AP' are constants, so we have the conclusion that $OC \cdot OP'$ is a constant. The second condition has been proved. If we place the modified Peaucellier linkage on the top of the linkage in Fig.2.11, making point O coincide, and using an extra

link to constraint the movement of point C on a circle, the point P' will move along the perfect vertical straight line $P'M'$ in Fig.2.11. The modified Peaucellier linkage is in a very compact form. This design was applied in the air engines which are employed to ventilate the House of Parliament.

Chapter 3

Linkage Synthesis Theory

In this chapter, some basic kinematics and linkage synthesis theories will be introduced. McCarthy has already presented these theories in [9] [8]. We summarize these theories in this chapter. We will start with the definition of coordinates transformation and homogeneous transformation. Since only planar linkages can be used in our MEMS suspension, here we focus more on the planar linkages. The motion of RR chain and 3R chain will be analyzed and the four-bar linkage synthesis theory will be introduced in this chapter.

3.1   Displacement

We will firstly focus on the coordinates transformation. If we want to know the relative position of two rigid bodies in space, we need to attach two coordinate frames to them. One of the frame is set as the ground frame F, the other will be set as the moving frame M. We denote the coordinates transformation as $D : F \rightarrow M$, which transform coordinates

measured in M to the frame in F. The transformation is denoted as:

$$\mathbf{X} = [A]\mathbf{x} + \mathbf{d} \tag{3.1}$$

where $\mathbf{x}$ is the coordinates measured in the moving frame M while $\mathbf{X}$ is the coordinates measured in the fixed frame F. If the rigid body is moving in a n dimensional space, then $[A]$ is a $n \times n$ matrix and $\mathbf{d}$ is a n dimensional vector. Specially, in planar cases $n = 2$, which makes $[A]$ a 2×2 matrix and $\mathbf{d}$ a 2 dimensional vector.

For the rigid body, the distance of any two different points on it should keep the same no matter in what reference frame. This is called the rigid body motion. Now let us derive the distance formula both in the moving fame and the fixed frame for two different points on the rigid body to get some insight for the matrix $[A]$.

Let us denote the coordinates of the two points in the fixed frame as P and Q. The distance for these two points is defined by the Euclidean distance formula which is as the following:

$$|P - Q| = \sqrt{(P - Q)^T(P - Q)} \tag{3.2}$$

Now let us denote the coordinates of the two points in the moving frame as p and q. From equation(3.1), we get

$$|P - Q| = |([A]p + d) - ([A]q + d)| = |[A](p - q)| \tag{3.3}$$

Using equation(3.2), we have

$$|P - Q| = \sqrt{(p - q)^T[A]^T[A](p - q)} \tag{3.4}$$

If we directly measure the distance in the moving frame M, we get

$$|p - q| = \sqrt{(p-q)^T(p-q)} \tag{3.5}$$

The distance is the same in both reference frame, so we have equation(3.4) equals to equation(3.7), from which we can get

$$[A]^T[A] = [I] \tag{3.6}$$

The square matrix satisfies equation(3.6) is called orthogonal matrix. And we can also get the determinant of $[A]$ as following:

$$det([I]) = det([A]^T[A]) = (det[A])^2 = 1 \tag{3.7}$$

So we have $det([A]) = 1$ or $det([A]) = -1$. Specially, when the determinant is equals to positive one, the matrix $[A]$ is called rotation matrix. In rigid body transformation, we focus on the matrices have positive one determinant.

A displacement in n dimensional space can be defined by $n \times n$ rotation matrix $[A]$ and n dimensional translation vector d. If d is zero, it is a pure rotation motion and if $[A]$ is zero, it is pure translation.

The displacement is not a linear transformation. We show it in the following. For pure translation, the translation of the sum of two vectors, x and y, by distance d is defined as the following:

$$T(x + y) = x + y + d \tag{3.8}$$

while the sum of the translation of each vector separately is defined as:

$$T(x) + T(y) = x + d + y + d = x + y + 2d \tag{3.9}$$

We have noticed, equation(3.8) is not equals to equation(3.9). The homogeneous transformation is defined as

$$\left\{ \begin{matrix} \mathbf{X} \\ 1 \end{matrix} \right\} = \left[\begin{matrix} A & \mathbf{d} \\ 0 & 1 \end{matrix} \right] \left\{ \begin{matrix} \mathbf{x} \\ 1 \end{matrix} \right\} \tag{3.10}$$

The $(n+1) \times (n+1)$ matrix $[T] = [A, d]$ is called homogeneous transformation matrix.

If the coordinates of a point P measured in the moving frame M is denoted as $\mathbf{x} = (x, y)$, then the coordinates of P measured in the fixed frame F by the definition of displacement can be obtained from equation(3.1). We denote $[A]$ and $\mathbf{d}$ as the following:

$$[\mathrm{A}] = \left[\begin{matrix} cos\theta & -sin\theta \\ sin\theta & cos\theta \end{matrix} \right], \quad \mathbf{d} = \left\{ \begin{matrix} d_1 \\ d_2 \end{matrix} \right\}$$

So we have

$$\left\{ \begin{matrix} X \\ Y \end{matrix} \right\} = \left[\begin{matrix} cos\theta & -sin\theta \\ sin\theta & cos\theta \end{matrix} \right] \left\{ \begin{matrix} x \\ y \end{matrix} \right\} + \left\{ \begin{matrix} d_1 \\ d_2 \end{matrix} \right\} \tag{3.11}$$

If we write it as the homogeneous form, we get

$$\left\{ \begin{matrix} X \\ Y \\ 1 \end{matrix} \right\} = \left[\begin{matrix} cos\theta & -sin\theta & d_1 \\ sin\theta & cos\theta & d_2 \\ 0 & 0 & 1 \end{matrix} \right] \left\{ \begin{matrix} x \\ y \\ 1 \end{matrix} \right\} \tag{3.12}$$

22

3.2 Analysis of RR Chain

The homogeneous transformation works very well for two coordinates system transformation. When it comes to robotic arm analysis, we usually decompose the motion to pure rotation and pure translation. We will use the Denavit-Hartenberg method to analyze the robotic manipulators here. The Denavit-Hartenberg method has the following format:

$$[T] = [Z_1][X_1][Z_2][X_2]...[X_{n-1}][Z_n] \tag{3.13}$$

where the Z matrix represents the rotation about the pivot and the X matrix represents the translation along the robot arm or the link. The RR robot is showing in Fig.3.1. The planar
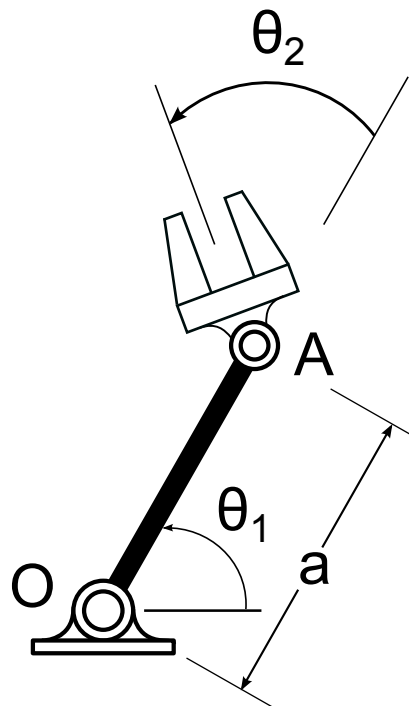
Figure 3.1: THE RR ROBOT.

RR chain robot has a fixed ground pivot O that connects a rotating link, or crank, to the ground link. The second revolute joint is A which connects the crank to the floating link.

We build the fixed frame, or world frame, with origin at point O. And the x axis of the fixed frame is along the zero position of link OA. The zero position of link OA is the case when the angle θ_1 is zero. The origin of moving frame is set at the second revolute joint A. The x axis direction of the moving frame is set initially along the direction of link OA. Then the coordinates of any point measured in the moving frame can be represented in the fixed frame by using the Denavit-Hartenberg method as following:

$$\mathbf{X} = [Z(\theta_1)][X(a)][Z(\theta_2)] \tag{3.14}$$

where a is the length of link OA. Write equation(3.14) in matrix form, we get

$$\begin{Bmatrix} X \\ Y \\ 1 \end{Bmatrix} = \begin{bmatrix} cos\theta_1 & -sin\theta_1 & 0 \\ sin\theta_1 & cos\theta_1 & 0 \\ 0 & 0 & 1 \end{bmatrix} \begin{bmatrix} 1 & 0 & a \\ 0 & 1 & 0 \\ 0 & 0 & 1 \end{bmatrix} \begin{bmatrix} cos\theta_2 & -sin\theta_2 & 0 \\ sin\theta_2 & cos\theta_2 & 0 \\ 0 & 0 & 1 \end{bmatrix} \begin{Bmatrix} x \\ y \\ 1 \end{Bmatrix} \tag{3.15}$$

We expand the equation(3.15) and make a simplification, we get the following:

$$\begin{Bmatrix} X \\ Y \\ 1 \end{Bmatrix} = \begin{bmatrix} cos(\theta_1 + \theta_2) & -sin(\theta_1 + \theta_2) & acos\theta_1 \\ sin(\theta_1 + \theta_2) & cos(\theta_1 + \theta_2) & asin\theta_1 \\ 0 & 0 & 1 \end{bmatrix} \begin{Bmatrix} x \\ y \\ 1 \end{Bmatrix} \tag{3.16}$$

Notice that the position of the end-effector is equivalent to the combination of a translation by vector $\mathbf{d} = (acos\theta_1, asin\theta_1)$ and a rotation by the angle $\varphi = \theta_1 + \theta_2$.

3.3 Analysis of 3R Chain

For the 3R chain, we have one more elbow revolute joint E between joint O and A. The link length OE is denoted as a_1 and the link length EA is denoted as a_2. The rotation angle
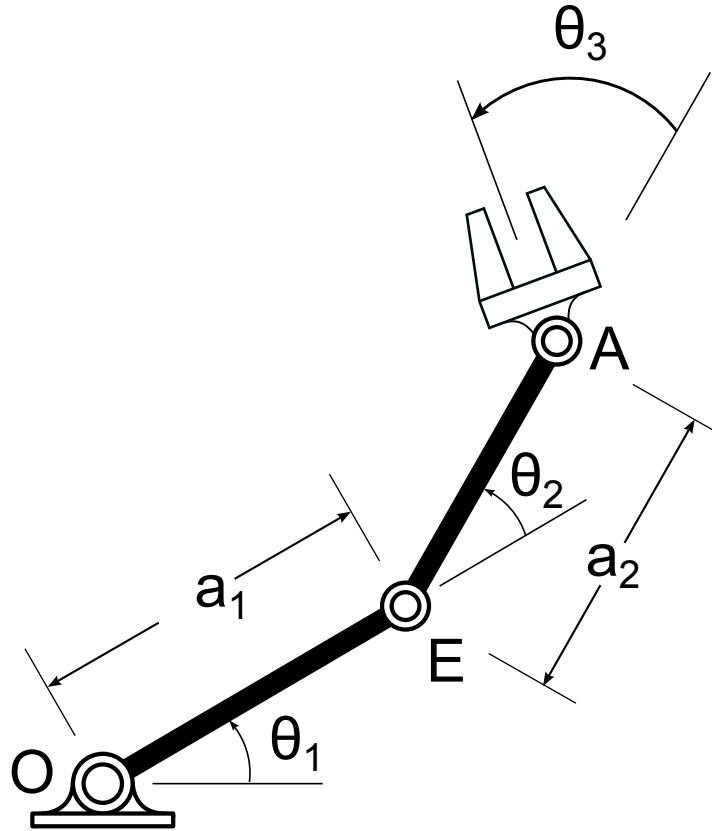
Figure 3.2: THE RRR ROBOT.

of the elbow joint E is measured from the link OA to the link EA. The rotation angle of
the end-effector around A is now θ_3 instead of θ_2 in the RR chain case. So we have the
kinematics equation for the RRR chain as following:

$$\mathbf{X} = [Z(\theta_1)][X(a_1)][Z(\theta_2)][X(a_2)][Z(\theta_3)] \tag{3.17}$$

Similarly, write equation(3.17) in matrix form, we get

$$
\begin{Bmatrix} X \\ Y \\ 1 \end{Bmatrix} = \begin{bmatrix} cos\theta_1 & -sin\theta_1 & 0 \\ sin\theta_1 & cos\theta_1 & 0 \\ 0 & 0 & 1 \end{bmatrix} \begin{bmatrix} 1 & 0 & a_1 \\ 0 & 1 & 0 \\ 0 & 0 & 1 \end{bmatrix} \begin{bmatrix} cos\theta_2 & -sin\theta_2 & 0 \\ sin\theta_2 & cos\theta_2 & 0 \\ 0 & 0 & 1 \end{bmatrix}
$$
$$
\cdot \begin{bmatrix} 1 & 0 & a_2 \\ 0 & 1 & 0 \\ 0 & 0 & 1 \end{bmatrix} \begin{bmatrix} cos\theta_3 & -sin\theta_3 & 0 \\ sin\theta_3 & cos\theta_3 & 0 \\ 0 & 0 & 1 \end{bmatrix} \begin{Bmatrix} x \\ y \\ 1 \end{Bmatrix}
$$
(3.18)

Expanding and simplifying equation(3.18) give us

$$
\begin{Bmatrix} X \\ Y \\ 1 \end{Bmatrix} = \begin{bmatrix} cos(\theta_1 + \theta_2 + \theta_3) & -sin(\theta_1 + \theta_2 + \theta_3) & a_1cos\theta_1 + a_2cos\theta_2 \\ sin(\theta_1 + \theta_2 + \theta_3) & cos(\theta_1 + \theta_2 + \theta_3) & a_1sin\theta_1 + a_2sin\theta_2 \\ 0 & 0 & 1 \end{bmatrix} \begin{Bmatrix} x \\ y \\ 1 \end{Bmatrix}
$$
(3.19)

Notice that the position of the end-effector is equivalent to the combination of a translation by vector $\mathbf{d} = (a_1cos\theta_1 + a_2cos\theta_2, a_1sin\theta_1 + a_2sin\theta_2)$ and a rotation by the angle $\varphi = \theta_1 + \theta_2 + \theta_3$.

3.4 Synthesis of Four-bar Linkage

The method of synthesis of four-bar linkage is starting from synthesis of a RR chain which can go through five task positions we specified. We first set up a fixed frame. Each of the five task positions is denoted by a rotation angle and a translation vector in the fixed frame. The homogeneous transformation matrix is defined as $[T(\phi_i, d_i)], i = 1, ..., 5$, where ϕ_i is the rotation angle and d_i is the translation vector. Let us denote the ground pivot as G and the joint on the other side of the crank as W. The coordinates of the ground pivot in the fixed frame is $G = (u, v)$ while the coordinates of the floating pivot in the moving frame is $w = (x, y)$. The w is a fixed point in the moving frame. From the knowledge of the previous

26

sections, we know the coordinates of the floating pivot in the fixed frame is

$$W^i = [T(\phi_i, d_i)]w \tag{3.20}$$

The synthesis problem is finding the point w in the end-effector, such that its fixed frame coordinates in each task position, $W^i, i = 1, ..., 5$ is around a fixed point G. The condition that the pivot W lie on a circle about G yields the equation that

$$(W - G) \cdot (W - G) = R^2 \tag{3.21}$$

where R is the distance between W and G. Using equation(3.20) we get

$$([T(\phi_i, d_i)]w - G) \cdot ([T(\phi_i, d_i)]w - G) = R^2, \qquad i = 1, ..., 5 \tag{3.22}$$

To simplify these equations, we use $W^1 = [T(\phi_1, d_1)]w$ as our design variables, instead of w, and make the substitution $w = [T(\phi_1, d_1)]^{-1}W^1$. We define the relative displacement as

$$[D_{1j}] = [T(\phi_i, d_i)][T(\phi_1, d_1)]^{-1} \quad i = 1, ..., 5 \quad j = 1, ..., 5 \tag{3.23}$$

Notice that $[D_{11}] = [I]$. We have a set of equations

$$(W^1 - G) \cdot (W^1 - G) = R^2 \tag{3.24}$$

$$([D_{12}]W^1 - G) \cdot ([D_{12}]W^1 - G) = R^2 \tag{3.25}$$

$$([D_{13}]W^1 - G) \cdot ([D_{13}]W^1 - G) = R^2 \tag{3.26}$$

$$([D_{14}]W^1 - G) \cdot ([D_{14}]W^1 - G) = R^2 \tag{3.27}$$

$$([D_{15}]W^1 - G) \cdot ([D_{15}]W^1 - G) = R^2 \tag{3.28}$$

The constraint equation are five equations with five unknowns $W^1 = (x, y)$, $G = (u, v)$ and R. So we can solve these five equations to determine the five unknowns. We can have at most four solutions by solving these equations. By picking any two sets of them, we have one design of four-bar linkage. Totally, we can have at most six four-bar linkage designs.

Chapter 4

Rectilinear Eight-bar Linkage

The method of synthesis of eight-bar linkages start from defining two 3R chain firstly and adding a RR chain constraint after, has already been presented by Soh and McCarthy (2007)[12]. Continuing research on finding all possible ways of applying the RR constraint was presented by Sonawale and McCarthy (2014)[13]. In our research, we specified the five task positions on a straight line. We followed the same procedure to get a number of eight-bar linkages.

Firstly we need to derive the kinematic equations of the planar 3R chain. Let [D] denote the homogeneous transformation from task frame to fixed frame. [G] is the transformation matrix from the 3R chain base to fixed frame. We define [H] as the transformation matrix from task frame to end-effector frame. The length of the 3 moving links were represented as a_1, a_2 and a_3 respectively. θ_1, θ_2 and θ_3 are relative rotation angles of each moving frame. Let Z denote the homogeneous transformation matrix of the moving frame. The homogeneous transformation matrix [D] can be denoted as

$$[D] = [G]Z(\theta_1, 0)Z(\theta_2, a_1)Z(\theta_3, a_2)[H]. \tag{4.1}$$

Five task positions have already been specified on a straight line so we can solve $(\theta_{1j}, \theta_{2j}, \theta_{3j}), j = 1, ..., 5$ for each of the five task positions using

$$[D_j] = [G]Z(\theta_{1j}, 0)Z(\theta_{2j}, a_1)Z(\theta_{3j}, a_2)[H], \quad j = 1, ..., 5. \tag{4.2}$$

The next step is defining two RR constraints between any two of the moving link. Let's define $[B_{lj}]$ to be the homogeneous transformation matrix of the l*th* moving link to the fixed frame and $[B_{kj}]$ to be the homogeneous transformation matrix of the k*th* moving link to the fixed frame. The l*th* moving link and the k*th* moving link are connected by a RR constraint link. The joint position, g, is where the RR constraint link connected the l*th* link measured in moving frame $[B_{lj}]$ and w is the joint position where RR constraint link connected the k*th* link measured in moving frame $[B_{kj}]$. In the process of the task frame moving through all the five task positions, the coordinates of two ends of the RR constraint link, measured in the fixed frame, are given by

$$G^j = [B_{lj}]g \quad and \quad W^j = [B_{kj}]w. \tag{4.3}$$

Relative displacement is introduced for convenient calculation

$$[R_{1j}] = [B_{lj}][B_{l1}]^{-1} \quad and \quad [S_{1j}] = [B_{kj}][B_{k1}]^{-1}. \tag{4.4}$$

Substitute equation (4.4) into equation (4.3) we get

$$G^j = [R_{1j}]G^1 \quad and \quad W^j = [S_{1j}]W^1. \tag{4.5}$$

Note that $[R_{11}] = [S_{11}] = [I]$ are identity matrix. The two ends of the RR constraint link were defined by G^j and W^j. Assuming the length of the RR constraint link is R so we can

get constraint equations for five take positions

$$([R_{1j}]G^1 - [S_{1j}]W^1]) \cdot ([R_{1j}]G^1 - [S_{1j}]W^1]) = R^2, \quad j = 1, ..., 5. \tag{4.6}$$

Here we get five constraint equations and five variables. We can solve for $G^1 = (u, v, 1)^T$, $W^1 = (x, y, 1)^T$ and R using the five task positions which have been specified on a straight line. The method of solving RR constraint equations of a four-bar linkage has been presented by McCarthy[9]. We used the same method here, subtracting the first of the five equations from the remaining four to reduce the total variables to four. By using Mathematica's *Nsolve* function, we can get all the possible eight-bar linkage designs satisfying our task position requirements.

Chapter 5

MEMS Implementation

MEMS fabrication requires single layer design. First, we need to find non-overlap eight-bar linkages from the numerous solutions we obtained from the above synthesis process. This requires all links of the eight-bar linkage must not overlap each other when the end-effector moves through all the five task positions. Here are two examples of overlap and non-overlap eight-bar linkages. The eight-bar linkage shown in Fig.5.1 is in overlap form. It can provide rectilinear motion but several links have to be placed on different layers to make the whole mechanism work. The one shown in Fig.5.2 is an example of non-overlap linkage.

The ones we obtained from the synthesis of eight-bar linkages are all in asymmetric shape. We redesigned the eight-bar linkage and made it perfectly symmetric due to the powerful advantages offered by symmetric shape in MEMS gyroscope application. The redesigned eight-bar linkage is shown in Fig.5.2.

After redesigning, the end effector still showed very good rectilinear property. After evaluating the rectilinear performance of the symmetric eight-bar linkage, we traced the motion path of the end-effector. The path can be seen in Fig.5.3, which is a perfect straight line just from observation. We extracted 253 points from the straight line and got the exact
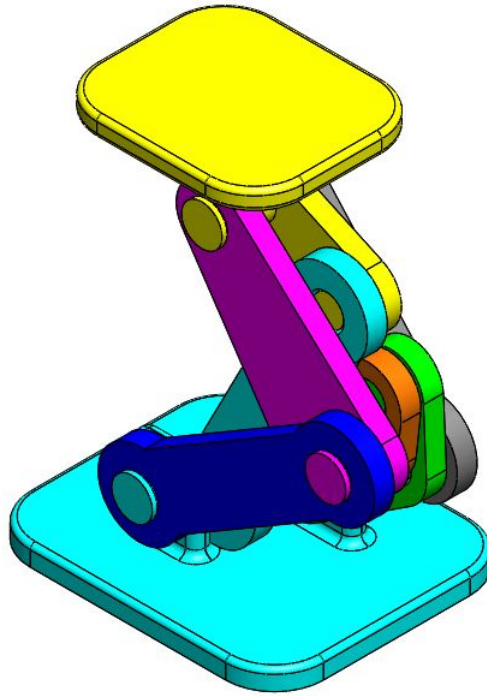
Figure 5.1: AN EXAMPLE OF A RECTILINEAR EIGHT-BAR LINKAGE WITH OVER-LAPPING LINKS.
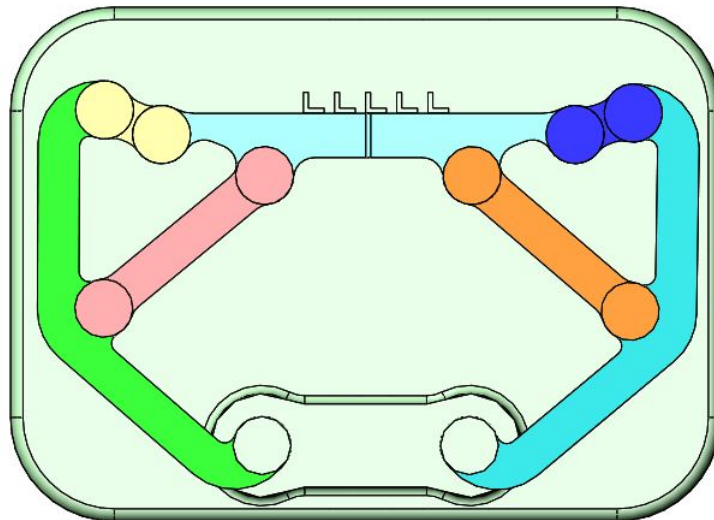
Figure 5.2: A SYMMETRIC RECTILINEAR EIGHT-BAR LINKAGE WITH NON-OVERLAPPING LINKS.
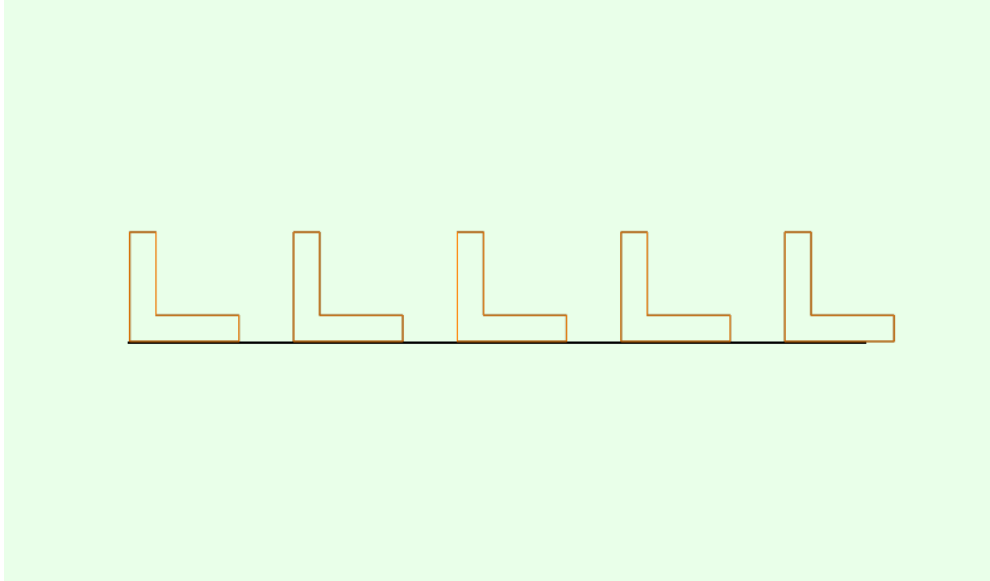
Figure 5.3: TRACING THE END-EFFECTOR PATH OF SYMMETRIC EIGHT-BAR LINKAGE.

Table 5.1: COORDINATES OF TRACING POINTS.

X(mm)	Y(mm)	Z(mm)
34.93411	-70.0572	21.11394
34.94115	-70.0572	21.11394
34.96226	-70.0572	21.11394
34.9974	-70.0571	21.11394
35.04651	-70.057	21.11394
35.10951	-70.0569	21.11394
35.18629	-70.0567	21.11394
35.27672	-70.0566	21.11394
35.38065	-70.0563	21.11394
35.4979	-70.0561	21.11394
35.62828	-70.0558	21.11394
35.77158	-70.0556	21.11394
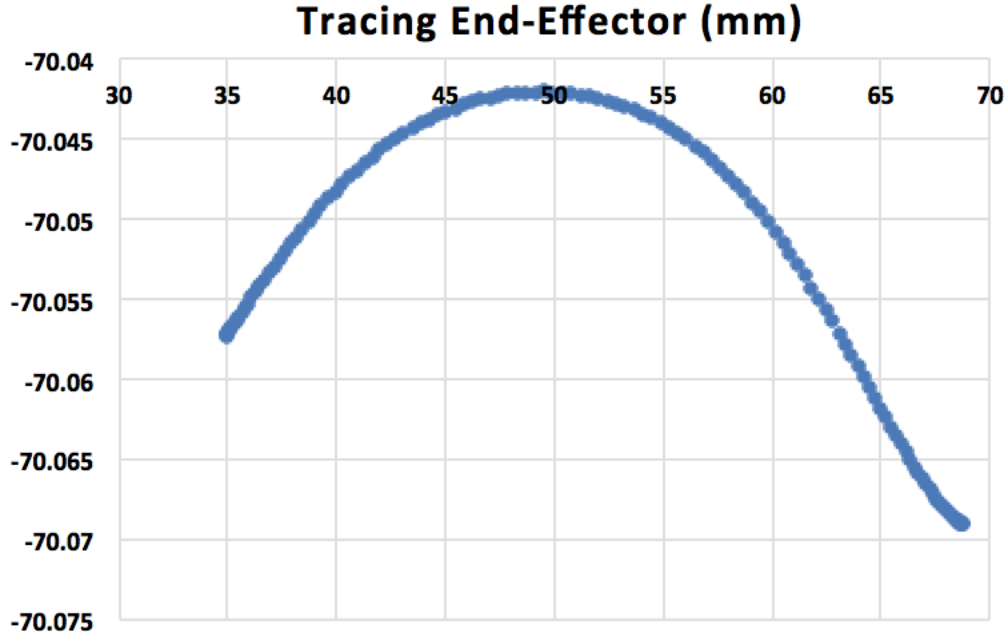
Figure 5.4: THE VERTICAL DEVIATION IS 0.03MM FOR A TRAVEL OF 30MM, WHICH IS 0.1% DEVIATION.

coordinates for each point. Part of the points coordinates are shown in Table.5.1 as an example. A curve shown in Fig.5.4 was created to show the 253 points. The X-axis and Y-axis represented the X coordinates and Y coordinates of each point. The total displacement in X-direction for the end-effector moved from the first task position to the fifth task position is 33.1 millimeters. During this process, the maximum and minimum Y coordinates of the tracing point were -70.042 millimeters and -70.069 millimeters respectively. The maximum deviation in the Y-direction of the end effector was only 0.027 millimeter while it went horizontally 33.1 millimeters. Here we analyzed the performance of the symmetric eight-bar linkage using millimeter units. We need to scale it to micron units during fabrication. We can see the redesigned symmetric eight-bar linkage manifested perfectly rectilinear motion property.

The next step was replacing all the rigid-body joints with flexure pivots. We used Finite-Element-Analysis method to evaluate the performance of the eight-bar flexure suspension
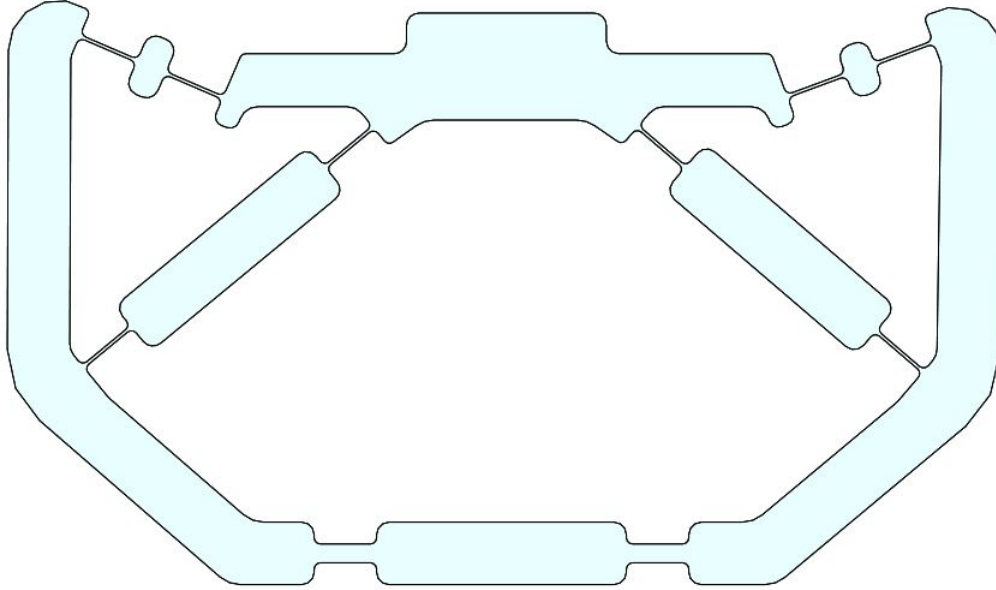
Figure 5.5: THE SYMMETRIC RECTILINEAR EIGHT-BAR LINKAGE WITH HINGES REPLACED WITH BEAM FLEXURES (FLEXURE SUSPENSION).

designed before. It turned out that the beam flexure at the joint position achieved the best result. From the Finite-Element-Analysis result, we refined the flexure suspension by changing the dimension of the flexure pivots. The base flexure pivots were made relatively thicker and shorter while the remaining joints used long thin beam flexure pivots. Finally, we obtained an eight-bar flexure suspension shown in Fig.5.5.

In Finite-Element-Analysis, we applied aluminum as the material of the eight-bar flexure suspension. The base link of the whole flexure suspension was fixed and horizontal force was applied at the end-effector. We used a curvature based mesh. The stress result is shown in Fig.5.6. The highest stress was observed at the two flexure pivots besides the base link. The displacement result is shown in Fig.5.7. The motion of the eight-bar flexure suspension was very close to the rigid-body solution. From the Finite-Element-Analysis result we can see the eight-bar flexure suspension has well-performed rectilinear motion property.
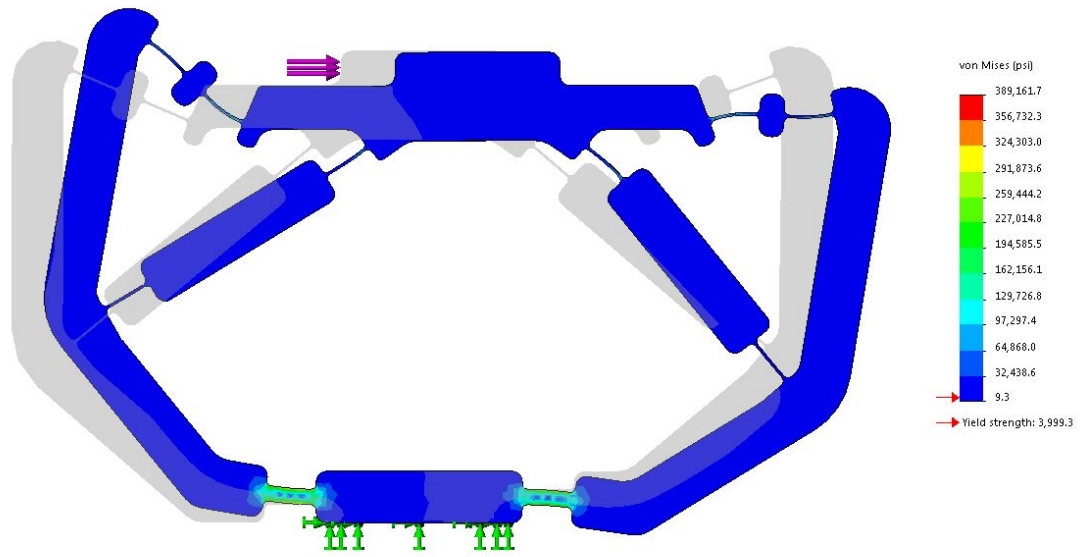
Figure 5.6: FINITE ELEMENT ANALYSIS SHOWING STRESSES IN THE EIGHT-BAR FLEXURE SUSPENSION.
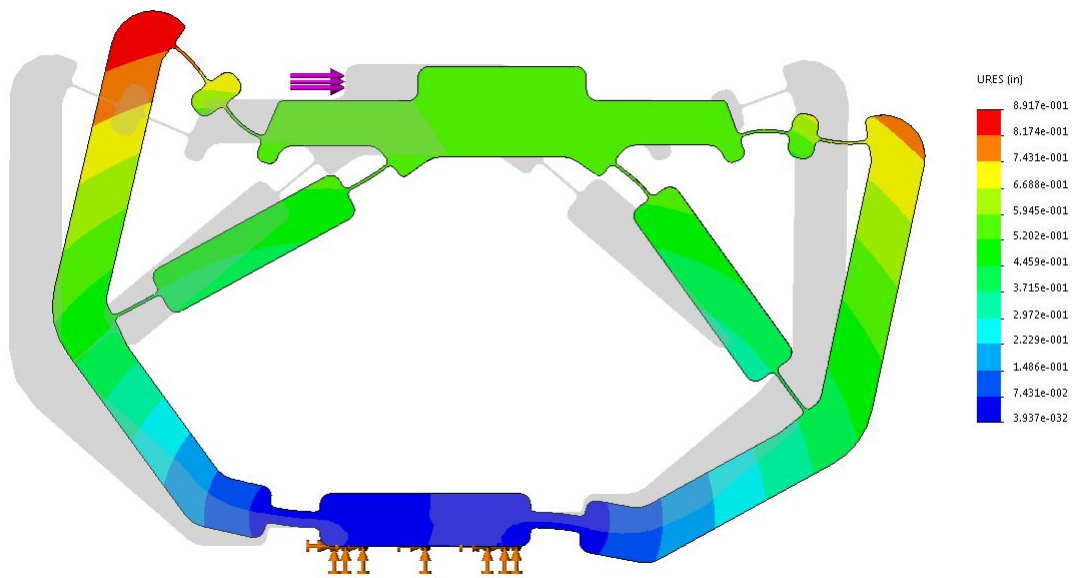
Figure 5.7: FINITE ELEMENT ANALYSIS SHOWING DISPLACEMENTS IN THE EIGHT-BAR FELXURE SUSPENSION.

Chapter 6

MEMS Gyroscope

The technology we used in MEMS gyroscope fabrication required the minimum beam width to be 3 microns and the gap width is between 0.7 micron and 50 microns. We need to scale our design to fit the fabrication rules in order to manufacture it. Different fabrication technology has different constraints. One example can been seen from[1, 15].

A driving linkage was designed to connect two sets of MEMS gyroscopes. Trusov et al. (2011)[14] has presented the conventional coupling mechanism used in MEMS gyroscope. The driving linkage in our research was constructed from two Chebyshevs Lambda linkages. The end-effector of Chebyshevs Lambda mechanism can go through straight line within a specific range. Part of one bar from eight-bar linkage was used as one link of the Chebyshevs Lambda linkage. We connect the end-effector of the two Chebyshevs Lambda linkages together to get our driving linkage. The model of the driving linkage connecting two eight-bar linkages is shown in Fig.6.1. The input was applied at the end-effector of the Chebyshevs Lambda linkage. Because of the rectilinear motion of the Chebyshevs Lambda linkages, the two eight-bar linkages can be driven to move in opposite directions, at the same time. An important MEMS gyroscope design rule is for small input to result in a large output so
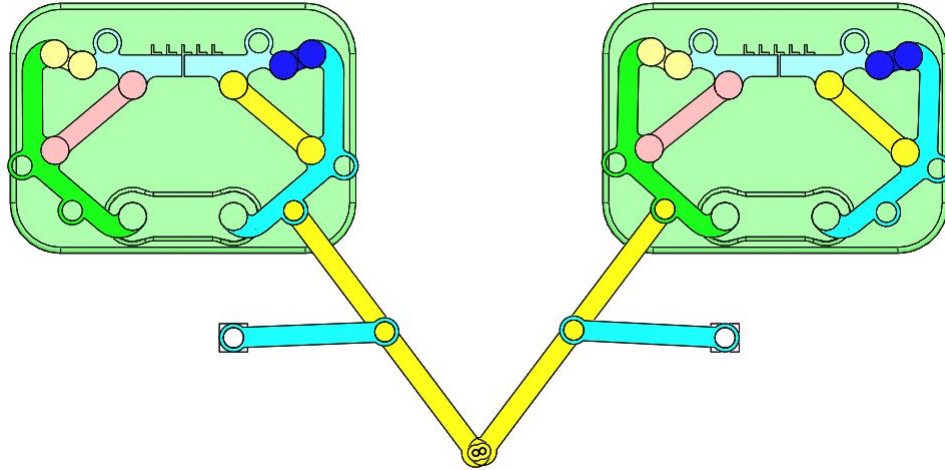
Figure 6.1: DESIGN OF A DRIVING LINKAGE FOR TWO EIGHT-BAR RECTILINEAR MOTION LINKAGES.

the driving linkage has to be made with high precision to achieve this goal. We transferred the rigid-body driving linkage to flexure pivots version as shown in Fig.6.2. Finite-Element-Analysis was conducted on evaluating the performance of the driving linkage. The displacement result is shown in Fig.6.3. We can see the two eight-bar flexure suspension moved in straight line validating the flexure pivots driving linkage performance.
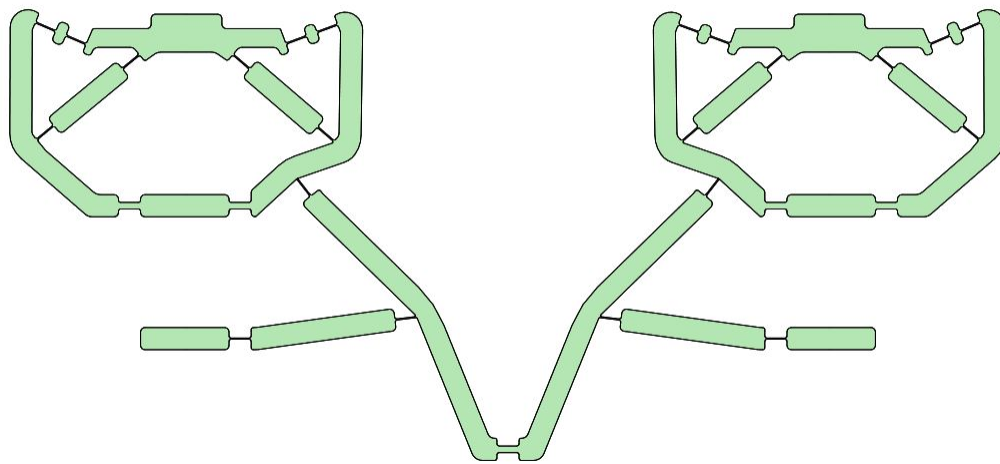
Figure 6.2: DESIGN OF THE DRIVING LINKAGE WITH HINGES REPLACED BY BEAM FLEXURES.
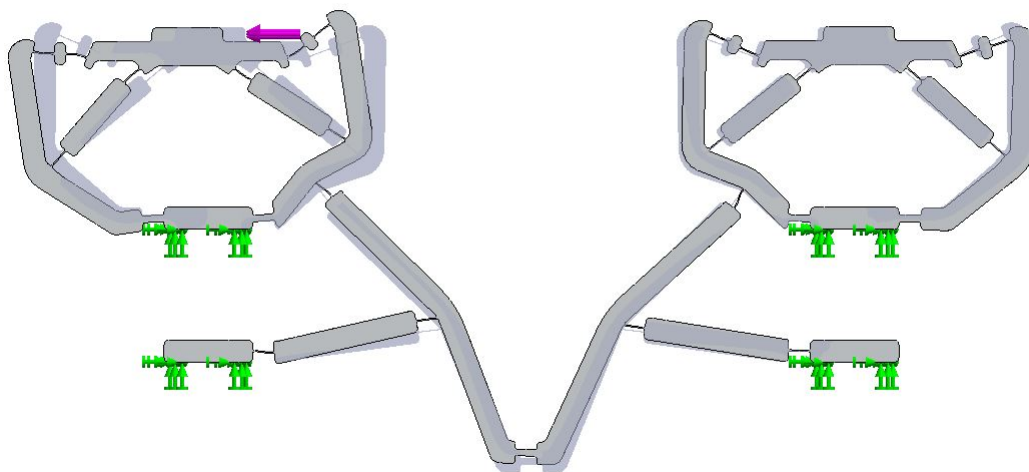
Figure 6.3: FINITE ELEMENT ANALYSIS SHOWING DISPLACEMENT OF THE DRIV-ING LINKAGE AND EIGHT-BAR FLEXURE SUSPENSION.

Chapter 7

Current Design

The long thin beam flexure pivots worked effectively in our current research. The whole MEMS gyroscope package included two sets of suspension connected by the driving linkage. Two examples of our current package design are shown in Fig.7.1 and Fig.7.2.
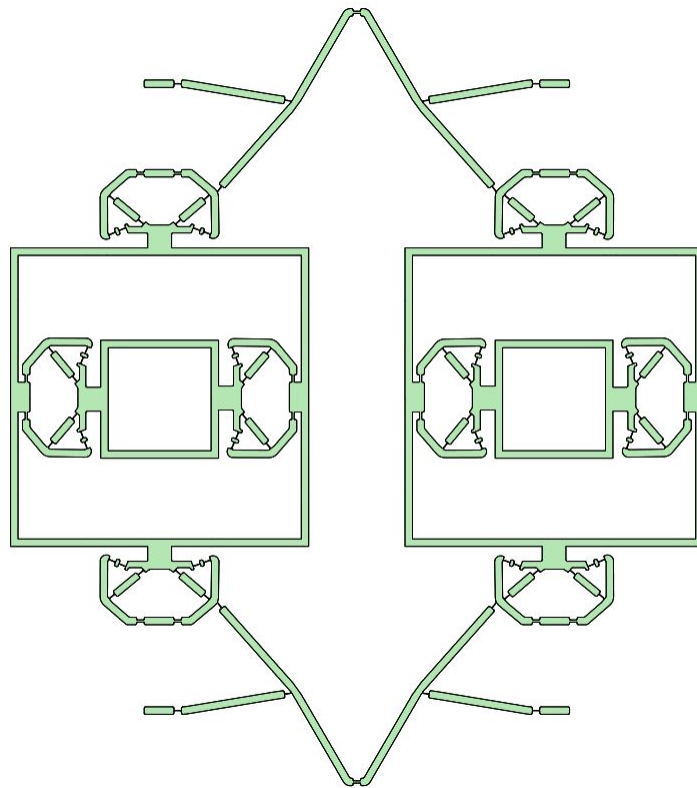
Figure 7.1: LAYOUT FOR A MEMS GYROSCOPE PROVIDING FLEXURES SUSPEN-
SIONS OF THE PROOF MASS IN TWO DIMENSIONS.
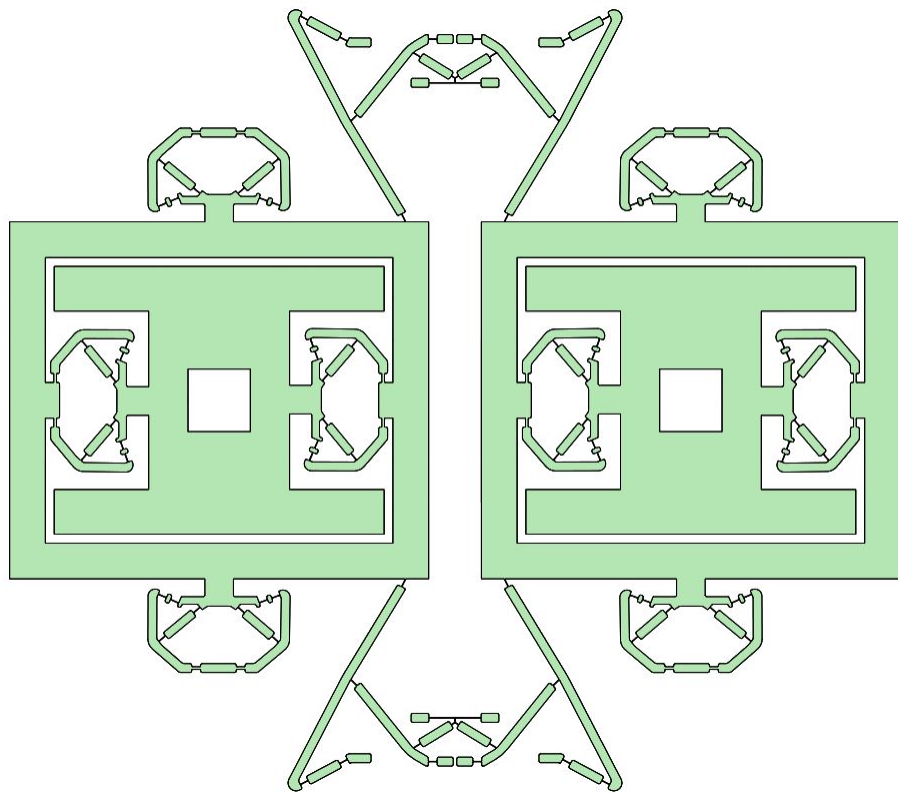
Figure 7.2: REVISED LAYOUT FOR A MEMS GYROSCOPE WITH A NEW DRIVING LINKAGE.

Chapter 8

Conclusion

In this paper, we present a symmetric flexure-connected eight-bar linkage designed to be a rectilinear suspension for the proof mass of a MEMS gyroscope. This rectilinear eight-bar linkage was designed with hinged pivots and then flexures were introduced and sized using Finite Element Analysis. The result is an eight-bar flexure suspension that provides 33 micrometers of travel end-to-end with a maximum 0.1% deviation of the end-effector path from a straight line.

Additional work will be to adjust the symmetric eight-bar flexure suspension to meet fabrication rules and verifying that the finished product achieves the predicted rectilinear properties. Fabrication of prototypes will verify the motion of this flexure-connected eight-bar linkage under the action of external forces. Further research and experimentation will be conducted to refine the design of this rectilinear MEMS suspension.

Bibliography

[1] S. E. Alper and T. Akin. A single-crystal silicon symmetrical and decoupled mems gyroscope on an insulating substrate. *Journal of Microelectromechanical Systems*, 14(4):707–717, 2005.

[2] S. Avadhanula and R. S. Fearing. Flexure design rules for carbon fiber microrobotic mechanisms. In *Robotics and Automation, 2005, ICRA 2005, Proceedings of the 2005 IEEE International Conference*, 2005.

[3] A. H. S. Awtar, Shorya and E. Sevincer. Characteristics of beam-based flexure modules. *Journal of Mechanical Design*, 129(6):625–639, 2007.

[4] L. L. Howell and A. Midha. A method for the design of compliant mechanisms with small-length flexural pivots. *Journal of Mechanical Design*, 116(1):280–290, 1994.

[5] L. L. Howell and A. Midha. Parametric deflection approximations for end-loaded, large-deflection beams in compliant mechanisms. *Journal of Mechanical Design*, 117(1):156–165, 1995.

[6] A. B. Kempe. *How to draw a straight line: a lecture on linkages.* Macmillan and Company, 1877.

[7] S. Kota. Design of compliant mechanisms: Applications to mems. In *1999 Symposium on Smart Structures and Materials*, 1999.

[8] J. M. McCarthy. *Introduction to theoretical kinematics.* MIT press, 1990.

[9] J. M. McCarthy and G. S. Soh. *Geometric design of linkages.* Springer, 2010.

[10] H. H. Pham and I.-M. Chen. Kinematics, workspace and static analyses of 2-dof flexure parallel mechanism. In *Proceeding of Control, Automation, Robotics and Vision, 2002, ICARCV 2002, 7th International Conference on Vol. 2. IEEE*, 2002.

[11] S. W. A. Q. Y. X. Shi, Qin and X. Ji. Design principle of suspension of mems gyroscope. In *Proceeding of Nano/Micro Engineered and Molecular Systems, 2006, NEMS'06, 1st IEEE International Conference on IEEE*, 2006.

[12] G. Soh and J. McCarthy. Synthesis of eight-bar linkages as mechanically constrained parallel robots. In *Proceeding of 12th IFToMM world congress A, Vol. 653*, 2007.

[13] K. H. Sonawale and J. M. McCarthy. Synthesis of useful eight-bar linkages as constrained 6r loops. In *Proceeding of ASME 2014 International Design Engineering Technical Conferences and Computers and Information in Engineering Conference*, 2014.

[14] I. P. P. S. A. Z. Trusov, Alexander A. and A. M. Shkel. Low-dissipation silicon tuning fork gyroscopes for rate and whole angle measurements. *Sensors Journal*, 11(11):2763–2770, 2011.

[15] H. Xie and G. K. Fedder. Fabrication, characterization, and analysis of a drie cmos-mems gyroscope. *Sensors Journal*, 3(5):622–631, 2003.

Appendices

A   Tracing Points Data

Table A.1: Tracing Points Data

X(mm)	Y(mm)	Z(mm)
34.93411	-70.0572	21.11394
34.94115	-70.0572	21.11394
34.96226	-70.0572	21.11394
34.9974	-70.0571	21.11394
35.04651	-70.057	21.11394
35.10951	-70.0569	21.11394
35.18629	-70.0567	21.11394
35.27672	-70.0566	21.11394
35.38065	-70.0563	21.11394
35.4979	-70.0561	21.11394
35.62828	-70.0558	21.11394
35.77158	-70.0556	21.11394

35.92758	-70.0552	21.11394
36.09603	-70.0549	21.11394
36.27668	-70.0545	21.11394
36.46925	-70.0542	21.11394
36.67346	-70.0538	21.11394
36.88902	-70.0534	21.11394
37.11562	-70.0529	21.11394
37.35296	-70.0525	21.11394
37.60072	-70.052	21.11394
37.85858	-70.0516	21.11394
38.12621	-70.0511	21.11394
38.40329	-70.0506	21.11394
38.68947	-70.0501	21.11394
38.98443	-70.0497	21.11394
39.28783	-70.0492	21.11394
39.59933	-70.0487	21.11394
39.91861	-70.0483	21.11394
40.24533	-70.0478	21.11394
40.57916	-70.0474	21.11394
40.91977	-70.0469	21.11394
41.26684	-70.0465	21.11394
41.62005	-70.0461	21.11394

41.97907	-70.0457	21.11394
42.3436	-70.0453	21.11394
42.71331	-70.045	21.11394
43.08791	-70.0446	21.11394
43.4671	-70.0443	21.11394
43.85056	-70.044	21.11394
44.23802	-70.0438	21.11394
44.62919	-70.0435	21.11394
45.02377	-70.0433	21.11394
45.42149	-70.0431	21.11394
45.82208	-70.0429	21.11394
46.22526	-70.0427	21.11394
46.63077	-70.0425	21.11394
47.03834	-70.0424	21.11394
47.44772	-70.0423	21.11394
47.85866	-70.0422	21.11394
48.2709	-70.0421	21.11394
48.68421	-70.0421	21.11394
49.09833	-70.0421	21.11394
49.51303	-70.042	21.11394
49.92808	-70.0421	21.11394
50.34325	-70.0421	21.11394

50.7583	-70.0421	21.11394
51.17301	-70.0422	21.11394
51.58717	-70.0423	21.11394
52.00054	-70.0424	21.11394
52.41293	-70.0426	21.11394
52.8241	-70.0428	21.11394
53.23386	-70.0429	21.11394
53.642	-70.0432	21.11394
54.0483	-70.0434	21.11394
54.45257	-70.0437	21.11394
54.8546	-70.044	21.11394
55.2542	-70.0443	21.11394
55.65116	-70.0446	21.11394
56.04531	-70.045	21.11394
56.43643	-70.0454	21.11394
56.82434	-70.0458	21.11394
57.20886	-70.0463	21.11394
57.5898	-70.0468	21.11394
57.96696	-70.0473	21.11394
58.34018	-70.0478	21.11394
58.70926	-70.0484	21.11394
59.07404	-70.049	21.11394

59.43433	-70.0496	21.11394
59.78996	-70.0502	21.11394
60.14076	-70.0508	21.11394
60.48656	-70.0515	21.11394
60.82719	-70.0522	21.11394
61.16249	-70.0528	21.11394
61.49229	-70.0535	21.11394
61.81644	-70.0542	21.11394
62.13477	-70.055	21.11394
62.44713	-70.0557	21.11394
62.75337	-70.0564	21.11394
63.05334	-70.0571	21.11394
63.3469	-70.0578	21.11394
63.63389	-70.0585	21.11394
63.91418	-70.0592	21.11394
64.18763	-70.0599	21.11394
64.45411	-70.0605	21.11394
64.71349	-70.0612	21.11394
64.96563	-70.0618	21.11394
65.21042	-70.0624	21.11394
65.44774	-70.063	21.11394
65.67746	-70.0635	21.11394

65.89947	-70.064	21.11394
66.11367	-70.0645	21.11394
66.31995	-70.065	21.11394
66.51821	-70.0654	21.11394
66.70835	-70.0658	21.11394
66.89028	-70.0662	21.11394
67.0639	-70.0666	21.11394
67.22914	-70.0669	21.11394
67.38591	-70.0672	21.11394
67.53413	-70.0674	21.11394
67.67374	-70.0677	21.11394
67.80466	-70.0679	21.11394
67.92683	-70.0681	21.11394
68.04019	-70.0682	21.11394
68.14469	-70.0684	21.11394
68.24027	-70.0685	21.11394
68.32688	-70.0686	21.11394
68.4045	-70.0687	21.11394
68.47307	-70.0688	21.11394
68.53256	-70.0689	21.11394
68.58295	-70.0689	21.11394
68.62422	-70.0689	21.11394

68.65633	-70.069	21.11394
68.67928	-70.069	21.11394
68.69305	-70.069	21.11394
68.69765	-70.069	21.11394
68.69305	-70.069	21.11394
68.67928	-70.069	21.11394
68.65633	-70.069	21.11394
68.62422	-70.0689	21.11394
68.58295	-70.0689	21.11394
68.53256	-70.0689	21.11394
68.47307	-70.0688	21.11394
68.4045	-70.0687	21.11394
68.32688	-70.0686	21.11394
68.24027	-70.0685	21.11394
68.14469	-70.0684	21.11394
68.04019	-70.0682	21.11394
67.92683	-70.0681	21.11394
67.80466	-70.0679	21.11394
67.67374	-70.0677	21.11394
67.53413	-70.0674	21.11394
67.38591	-70.0672	21.11394
67.22914	-70.0669	21.11394

67.0639	-70.0666	21.11394
66.89028	-70.0662	21.11394
66.70835	-70.0658	21.11394
66.51821	-70.0654	21.11394
66.31995	-70.065	21.11394
66.11367	-70.0645	21.11394
65.89947	-70.064	21.11394
65.67746	-70.0635	21.11394
65.44774	-70.063	21.11394
65.21042	-70.0624	21.11394
64.96563	-70.0618	21.11394
64.71349	-70.0612	21.11394
64.45411	-70.0605	21.11394
64.18763	-70.0599	21.11394
63.91418	-70.0592	21.11394
63.63389	-70.0585	21.11394
63.3469	-70.0578	21.11394
63.05334	-70.0571	21.11394
62.75337	-70.0564	21.11394
62.44713	-70.0557	21.11394
62.13477	-70.055	21.11394
61.81644	-70.0542	21.11394

61.49229	-70.0535	21.11394
61.16249	-70.0528	21.11394
60.82719	-70.0522	21.11394
60.48656	-70.0515	21.11394
60.14076	-70.0508	21.11394
59.78996	-70.0502	21.11394
59.43433	-70.0496	21.11394
59.07404	-70.049	21.11394
58.70926	-70.0484	21.11394
58.34018	-70.0478	21.11394
57.96696	-70.0473	21.11394
57.5898	-70.0468	21.11394
57.20886	-70.0463	21.11394
56.82434	-70.0458	21.11394
56.43643	-70.0454	21.11394
56.04531	-70.045	21.11394
55.65116	-70.0446	21.11394
55.2542	-70.0443	21.11394
54.8546	-70.044	21.11394
54.45257	-70.0437	21.11394
54.0483	-70.0434	21.11394
53.642	-70.0432	21.11394

53.23386	-70.0429	21.11394
52.8241	-70.0428	21.11394
52.41293	-70.0426	21.11394
52.00054	-70.0424	21.11394
51.58717	-70.0423	21.11394
51.17301	-70.0422	21.11394
50.7583	-70.0421	21.11394
50.34325	-70.0421	21.11394
49.92808	-70.0421	21.11394
49.51303	-70.042	21.11394
49.09833	-70.0421	21.11394
48.68421	-70.0421	21.11394
48.2709	-70.0421	21.11394
47.85866	-70.0422	21.11394
47.44772	-70.0423	21.11394
47.03834	-70.0424	21.11394
46.63077	-70.0425	21.11394
46.22526	-70.0427	21.11394
45.82208	-70.0429	21.11394
45.42149	-70.0431	21.11394
45.02377	-70.0433	21.11394
44.62919	-70.0435	21.11394

44.23802	-70.0438	21.11394
43.85056	-70.044	21.11394
43.4671	-70.0443	21.11394
43.08791	-70.0446	21.11394
42.71331	-70.045	21.11394
42.3436	-70.0453	21.11394
41.97907	-70.0457	21.11394
41.62005	-70.0461	21.11394
41.26684	-70.0465	21.11394
40.91977	-70.0469	21.11394
40.57916	-70.0474	21.11394
40.24533	-70.0478	21.11394
39.91861	-70.0483	21.11394
39.59933	-70.0487	21.11394
39.28783	-70.0492	21.11394
38.98443	-70.0497	21.11394
38.68947	-70.0501	21.11394
38.40329	-70.0506	21.11394
38.12621	-70.0511	21.11394
37.85858	-70.0516	21.11394
37.60072	-70.052	21.11394
37.35296	-70.0525	21.11394

37.11562	-70.0529	21.11394
36.88902	-70.0534	21.11394
36.67346	-70.0538	21.11394
36.46925	-70.0542	21.11394
36.27668	-70.0545	21.11394
36.09603	-70.0549	21.11394
35.92758	-70.0552	21.11394
35.77158	-70.0556	21.11394
35.62828	-70.0558	21.11394
35.4979	-70.0561	21.11394
35.38065	-70.0563	21.11394
35.27672	-70.0566	21.11394
35.18629	-70.0567	21.11394
35.10951	-70.0569	21.11394
35.04651	-70.057	21.11394
34.9974	-70.0571	21.11394
34.96226	-70.0572	21.11394
34.94115	-70.0572	21.11394
34.93411	-70.0572	21.11394